USCAP

ARTICLE

Arctigenin alleviates myocardial infarction injury through inhibition of the NFAT5-related inflammatory phenotype of cardiac macrophages/monocytes in mice

Shi-Hao Ni[1,2,3] · Shu-Ning Sun[1,2,3] · Zheng Zhou[1,2,3] · Yue Li[1,2,3] · Yu-Sheng Huang[1,2,3] · Huan Li[1,2,3] · Jia-Jia Wang[1,2,3] · Wei Xiao[4] · Shao-Xiang Xian[1,2,3] · Zhong-Qi Yang[1,2,3] · Ling-Jun Wang[1,2,3] · Lu Lu [1,2,3]

Abstract

In this study, we screened potential natural compounds for the treatment of myocardial infarction (MI) and explored the underlying mechanisms. We built three machine learning models to screen the potential compounds. qPCR, flow cytometry, immunohistochemistry, and immunofluorescence analyses were applied to analyze the pharmacological effects of the compounds on macrophages/monocytes in vivo and in vitro. Arctigenin (AG) was selected as a candidate, and echocardiography, Masson's trichrome staining, and TUNEL staining were utilized to detect the effect of AG on MI in vivo. Transcriptome analysis and subsequent bioinformatics analyses were performed to predict the target of the selected compound. Western blot and luciferase reporter assays were used to confirm the target and mechanism of AG. The reversibility of the effects of AG were verified through overexpression of NFAT5. The results showed that AG can improve cardiac injury after MI by reducing infarct size, improving heart function, and inhibiting cardiac death. In addition, AG suppresses inflammatory macrophages/monocytes and proinflammatory cytokines in vivo and in vitro. Transcriptomic and biological experiments revealed that AG modulates macrophage polarization via the NFAT5-induced signaling pathway. Therefore, our data suggest that AG can improve MI by inhibiting the inflammatory phenotype of macrophages/monocytes through targeting of NFAT5.

✉ Ling-Jun Wang
smu868@gzucm.edu.cn

✉ Lu Lu
coinland@gzucm.edu.cn

[1] The First Affiliated Hospital, Guangzhou University of Chinese Medicine, Guangzhou 510407, China

[2] Lingnan Medical Research Center, Guangzhou University of Chinese Medicine, Guangzhou 510407, China

[3] Key Laboratory of Chronic Heart Failure, Guangzhou University of Chinese Medicine, Guangzhou 510407, China

[4] School of Traditional Chinese Medicine, Southern Medical University, Guangzhou 510515, China

Introduction

Myocardial infarction (MI) can lead to permanent myocardial injury or death, and collagen scars form at MI sites [1, 2]. MI can result in heart failure, and it is one of the major determinants of morbidity and mortality worldwide [3]. With the development of thrombolytic therapy and angioplasty, the mortality of MI patients has significantly decreased. However, death after post-MI heart failure still occurs in ~10% of cases each year [4]. Thus, it is important to develop effective therapeutic strategies to preserve cardiac function after MI.

The extent of postinfarction remodeling relies on the size of the infarct area and the quality of cardiac repair [5, 6]. Excessive and prolonged inflammatory reactions may increase cardiomyocyte death and infarct size. Macrophages play key roles during both the initiation and inhibition of inflammation through subgroup polarization [7, 8]. Previous studies have shown that macrophages shift from inflammatory phenotypes to reparative phenotypes in the early stage after MI and can prevent excessive inflammatory

reactions in the context of severe cardiac pathology, suggesting that shifting macrophage phenotypes may be a strategy to improve cardiac function after MI [9, 10].

Many clinical studies in China have revealed that traditional Chinese medicine can improve MI and regulate immunity [11–13]. However, uncertainty regarding the compositions and mechanisms of these drugs limits their further development. In previous studies, we focused on discovering new drugs from among natural products and established a strategy for virtual screening of drugs through machine learning [14]. Here, we used our previously designed strategy to screen for active molecules for MI treatment in silico, in vitro and in vivo.

Methods

Small molecules and cell preparation

Arctigenin (AG) and other natural molecules were purchased from Chengdu Sanherb Biotech Co., Ltd (Chengdu, China). Monocytes (THP-1, human) and macrophages (RAW264.7, mouse) were purchased from the Cell Bank of the Chinese Academy of Sciences. Mouse cardiomyocytes were isolated from 1-day-old C57BL/6 mice using enzymatic digestion (0.8 mg/mL pancreatin, 125 unit/mL collagenase, and 2% antibiotics/antimycotics). Mouse heart pieces were digested with stirring for 10 min, and the supernatant was then collected. The different cell types were isolated by Percoll gradient separation (top Percoll layer: 55%; bottom Percoll layer: 65%). We collected the intermediate layer according to the protocol of Bing Wang at Monash University [15]. The cells were cultured in RPMI 1640 medium containing 10% fetal bovine serum and 1% streptomycin/penicillin and incubated at 37 °C with 5% CO_2. (see Supplementary procedures for further detail).

Cell viability assay

Cell viability was measured by the cell counting kit-8 (CCK-8) method. Briefly, RAW264.7 cells and mouse cardiomyocytes were seeded in 96-well plates with 1×10^4 cells per well. At the indicated timepoints, the medium was discarded, and new cell culture medium was added. Ten microliters of CCK-8 solution was added to the plate, and the plate was read at a wavelength of 450 nm in a microplate reader (Thermo Scientific, USA). The viability was calculated as follows: viability $(\%) = [(As-Ab)/(Ac-Ab)] \times 100\%$, where As is the absorbance of the experimental group, Ac is the absorbance of the control group, and Ab is the absorbance of the blank group, which contained only 10% CCK-8 solution dissolved in fresh culture medium.

Animal experiments

Six-week-old male C57BL/6 mice with body weights of 23 ± 1 g were obtained from the Guangzhou University of Chinese Medicine (certification no. SCXK (Yue) 2015-0167). For in vivo studies, the animals were randomly assigned to different groups ($n = 20$ per group). Blind methods were applied to collect and evaluate data from all experiments. All of our animal experiments were performed in accordance with the Guide for the Care and Use of Laboratory Animals and were approved by the Ethics Committee of Guangzhou University of Chinese Medicine (approval number: 20180122003).

Based on our previous experiment [16], the anterior descending coronary artery was ligated. After administering anesthesia and opening the chest, the left anterior descending coronary artery was ligated, and the chest was then closed. AG was administered daily at a dose of 2 mg/kg by intraperitoneal injection starting 2 h or 3 days after operation for 18 continuous weeks. The dosage was based on a previous report and our pharmacokinetic results [17] showing that the peak concentration (Cmax) of AG in plasma after this dose is ~1.56 μM, which achieves an effective concentration in vitro (1 μM) (Fig. S3).

Prediction of potential small molecules

To screen for small molecules involved in the suppression of IL-6 and TNF-α in silico, three algorithm models (neural network, support vector machine, and random forest models) were built according our previous protocol [14]. Machine learning was executed and optimized through the Caret package and Rcpi package based on the R program. Briefly, the training set contained 4797 samples (2056 active and 2741 inactive) for TNF-α and 334 samples (123 active and 211 inactive) for IL-6, which were collected from PubChem BioAssay and a literature search. A total of 4511 molecular features, including Molecular ACCess System (MACCS) keys, electrotopological state indices, and PubChem molecular fingerprints, were used to describe the molecules with the Rcpi package. The Boruta package was used to select relevant features. Receiver operating characteristic (ROC) methods were performed to evaluate the model parameter optimization after tenfold cross-validation. Then, we screened for potential molecules based on the models from our chemical library, which contained 1190 small molecules. We selected compounds that met both of the following conditions: (1) at least one of the three machine learning models for each cytokine (IL-6 and TNF-α) obtained a positive result (>0.5), and (2) two types of models (IL-6 and TNF-α) obtained positive results simultaneously.

Transcriptome and data analysis

Macrophages (RAW264.7 cells) were treated with vehicle (Con group), 0.5 mg/mL lipopolysaccharide (LPS) alone (LPS group) or 0.5 mg/mL LPS combined with 1 μM AG (LPS + AG group) for 24 h. Then, an RNA extraction kit (Qiagen, Germany) was utilized to extract total mRNA from the cells. Transcriptome analysis was performed using a HiSeq X Ten instrument by OE Biotech. Co., Ltd. (Shanghai, China). The hierarchical indexing for spliced alignment of transcripts 2 program was used to map the sequenced reads to the mm9 genome [18]. In the RefSeq mm9 annotation, HT-Seq counts were used to quantify the read counts of the RNA-Seq data and to subsequently align the reads to the exonic regions of genes. Gene set enrichment analysis (GSEA) was performed to analyze mRNA expression levels based on the Kyoto Encyclopedia of Genes and Genomes (KEGG) database and immunologic signatures of the Molecular Signatures Database (MSigDB). T-distributed stochastic neighbor embedding (t-SNE) was used to inspect the gene set clusters. Each experiment had three replicates.

Hypoxia model in vitro

A hypoxia model was established according to the methods in previous experiments [19]. Briefly, mouse primary cardiomyocytes were cultured in DMEM/F12 medium covered with mineral oil for 2 h (the mineral oil established hypoxia by isolating the medium from oxygen), and RAW264.7 cells were pretreated with 0.2 mg/mL LPS/AG for 12 h. Then, the RAW264.7 cells and cardiomyocytes were cocultured in a transwell chamber for 12 h before analysis (the RAW264.7 cells were cultured on the upper layer, which could be moved).

Flow cytometry analysis

Apoptosis analysis was carried out using a BD Biosciences kit (USA). In brief, the cells were incubated with annexin V-FITC and propidium iodide for 15 min. After washing, the cells were analyzed by a flow cytometer. The gating strategy was based on the control group, and the counts in Q2 or Q4 were considered apoptotic cells.

To analyze immunomarkers, the cells were suspended in PBS with 0.5% serum and stained with fluorescent antibodies (eBioscience, Inc., San Diego, USA) against CD86 (Cat. No. 740501), CD206 (Cat. No. 565250), CCR2 (Cat. No. 235983), F4/80 (Cat. No. 565410), and CD14 (Cat. No. 553739). Then, cytometric analysis or sorting was performed by a flow cytometer (MoFlo Astrios EQ, Beckman Coulter, Indianapolis, IN, USA). All the results from flow cytometry were analyzed with Summit Software Version 5.2 (Beckman).

Echocardiography

At 9 days and 28 days after surgery, echocardiography was performed using a Vevo 2100 Imaging System (VisualSonics Inc., Toronto, Canada). The ejection fraction (EF) was calculated according to the left ventricular internal diameters at end-diastole and end-systole, which were measured vertically on the long axis of the ventricle. All parameters were automatically obtained using the LV Trace measurement tool in the Cardiac Package and the Short Axis module in Vevo 2100 analysis software. The measurements were performed using a single-blinded method.

Histochemistry and immunofluorescence

Histology and cell staining for immunohistochemistry were performed on heart tissue that had been harvested, fixed in 4% paraformaldehyde, embedded in paraffin, and sliced into sections. After dewaxing of the sections, nonspecific peroxidase was blocked by treating the sections with 3% H_2O_2 for 15 min, after which the sections were washed with PBS. The samples were then covered with 5% BSA for 0.5 h and incubated with antibodies (anti-CD14, 1:200; Abcam, Cat. No. ab182032) at 4 °C overnight. The samples were then immunostained with HRP-conjugated antibodies (Abcam, Cat. No. ab131368) for 4 h at room temperature.

For immunofluorescence, cells were fixed with 4% paraformaldehyde for 15 min and blocked with 5% BSA for 0.5 h. After washing, the cells and paraffin-embedded tissue sections were incubated with fluorescently labeled anti-LyC6 antibodies (1:200, Abcam, Cat. No. ab15686).

Masson's trichrome staining was performed for infarct size analysis. The infarct size was measured as the percentage of infarct area vs. the left ventricle area. Staining was observed using a Leica fluorescence microscope (Leica, Germany). Quantification of all data was performed with ImageJ software.

Western blotting

The protein content was quantified by the BCA method, and 100 μg per sample was loaded onto 12% SDS polyacrylamide gels. After electrophoresis, the proteins were transferred to polyvinylidene fluoride (PVDF) membranes, which were blocked with 5% BSA and probed with primary antibodies (Affinity, 1:1000, phospho-JAK2 (Tyr1007, Cat. No. AF3022), phospho-STAT1 (Tyr701, Cat. No. AF3300), phospho-p65 (Ser536, Cat. No. AF2006), and phospho-IKb (Ser32/Ser36, Cat. No. AF2002); Abcam, 1:5000, anti-mouse GAPDH (Cat. No. ab181602)). After washing, the

PVDF membranes were incubated with a secondary antibody (Affinity, 1:2000, Cat. No. S0001) for 2 h. Finally, the blots on the membranes were scanned with a charge-coupled device (CCD) system (ImageStation 2000 MM, Kodak, USA).

Real-time fluorescence quantitative PCR (qPCR)

The TRIzol method was used to extract total RNA from cells (Life Technologies, USA). A cDNA Synthesis Kit (Takara, Japan) was used to synthesize cDNA for real-time fluorescence qPCR assays. PCR amplification was carried out on a thermal cycler in a reaction volume of 20 μL containing SYBR Green (Takara, Japan) using a MyiQ real-time PCR detection system (Bio-Rad). The data were analyzed using the $2^{-\Delta\Delta Ct}$ method, and the gene primers are listed in Table S1.

Luciferase reporter

We assayed the transcriptional activity of NFAT5 by luciferase reporter assay. The pGM-NFAT5-Luc reporter, which contains two NFAT5 binding motifs, and the pGME2F-SEAP reporter (used as a control reporter) were kindly provided by Dr Niu Wenbo. RAW247.6 cells were cultured in 24-well plates and then transfected with 200 ng of pGM-NFAT5-Luc and 20 ng of pGME2F-SEAP (1×10^6 cells/well). After 24 h, the cells were lysed, and the luciferase activity was measured with a Dual-Luciferase Reporter kit (Madison, WI, USA).

Lentivirus transfection

The consensus coding sequence of NFAT5 (CCDS22648.2, NM_018823.2) and lentiviruses were synthesized and purchased from GenePharma (Shanghai, China). The virus stocks were titrated by transduction of RAW264.7 cells to 1×10^7 TU/mL. For cell transfection, RAW264.7 cells were transfected with an NFAT5 overexpression lentivirus (lentivirus-OE-NFAT5) or a control lentivirus (lentivirus control) in 5 μg/mL polybrene. After selection via puromycin treatment, stable cell lines were established.

For mouse transfection, 200 μL of lentivirus-OE-NFAT5 or lentivirus control was injected into the tail vein, and NFAT5 protein expression in the mouse heart was then validated by western blotting.

Statistics

Bioinformatics data were analyzed using the R program (3.5.2, Austria) and Bioconductor packages (GeneAnswers, Rtsne, and Limma). GraphPad Prism Software 7.0 (CA, USA) was used for statistical analysis. The data are presented as the mean ± SD and were analyzed by one-way ANOVA. A post hoc Tukey's HSD test was performed when the ANOVA found significant interactions between variables. A P value or FDR q value <0.05 was considered to indicate statistical significance.

Results

AG is predicted to suppress IL-6 and TNF-α

First, we screened for inhibitors of TNF-α and IL-6 and built three machine learning models. The verification results and model parameters are shown in Fig. S1. All areas under the ROC curves of our models were greater than 0.85 according to the results of a random tenfold cross-validation (Fig. 1a). In the two models for TNF-α and IL-6, a compound was identified as positive if the possibility was more than 50%. Seven molecules from our chemical library passed the filtering criteria after screening (Fig. 1b). Then, we detected IL-6 and TNF-α mRNA levels by qPCR after treatment with each of the six molecules at a concentration of 2 μM. The results showed that AG was the best potential molecule with regard to antiinflammatory function (Fig. S2 and Fig. 1c). The CCK-8 data showed that macrophages (RAW264.7 cells) may be more sensitive to AG cytotoxicity than cardiomyocytes (primary culture) ($P < 0.001$). After 1 μM AG treatment for 12 h, the cell viability of macrophages decreased to 82.20% of baseline levels, while that of cardiomyocytes decreased to 97.77% of baseline levels (Fig. 1d). The qPCR data showed that 1 μM AG with 0.2 mg/mL LPS treatment significantly decreased the mRNA levels of IL-6 and that 1 μM AG with or without 0.2 mg/mL LPS treatment significantly decreased the mRNA levels of TNF-α ($P < 0.05$). There were no marked effects of 1 μM AG on IL-10 expression (Fig. 1e).

AG modulates macrophage polarization in vitro

To investigate the effects of AG on macrophage polarization, we detected the levels of M1 (CD86) and M2 (CD206) markers in macrophages (RAW264.7 cells) with/without 0.2 mg/mL LPS stimulation by flow cytometry. Our results showed that LPS significantly increased the levels of both CD86 and CD206 ($P < 0.05$). It is possible that LPS polarizes macrophages directly toward the M1 phenotype and indirectly toward the M2 phenotype by driving Th2 cytokine expression. Compared with LPS, AG significantly decreased the levels of CD86 ($P < 0.05$). Furthermore, AG also increased CD206 levels in cells with or without 0.2 mg/mL LPS treatment (Fig. 2a). The immunofluorescence results also showed that AG regulated macrophage polarization, consistent with the flow cytometry results (Fig. 2b).
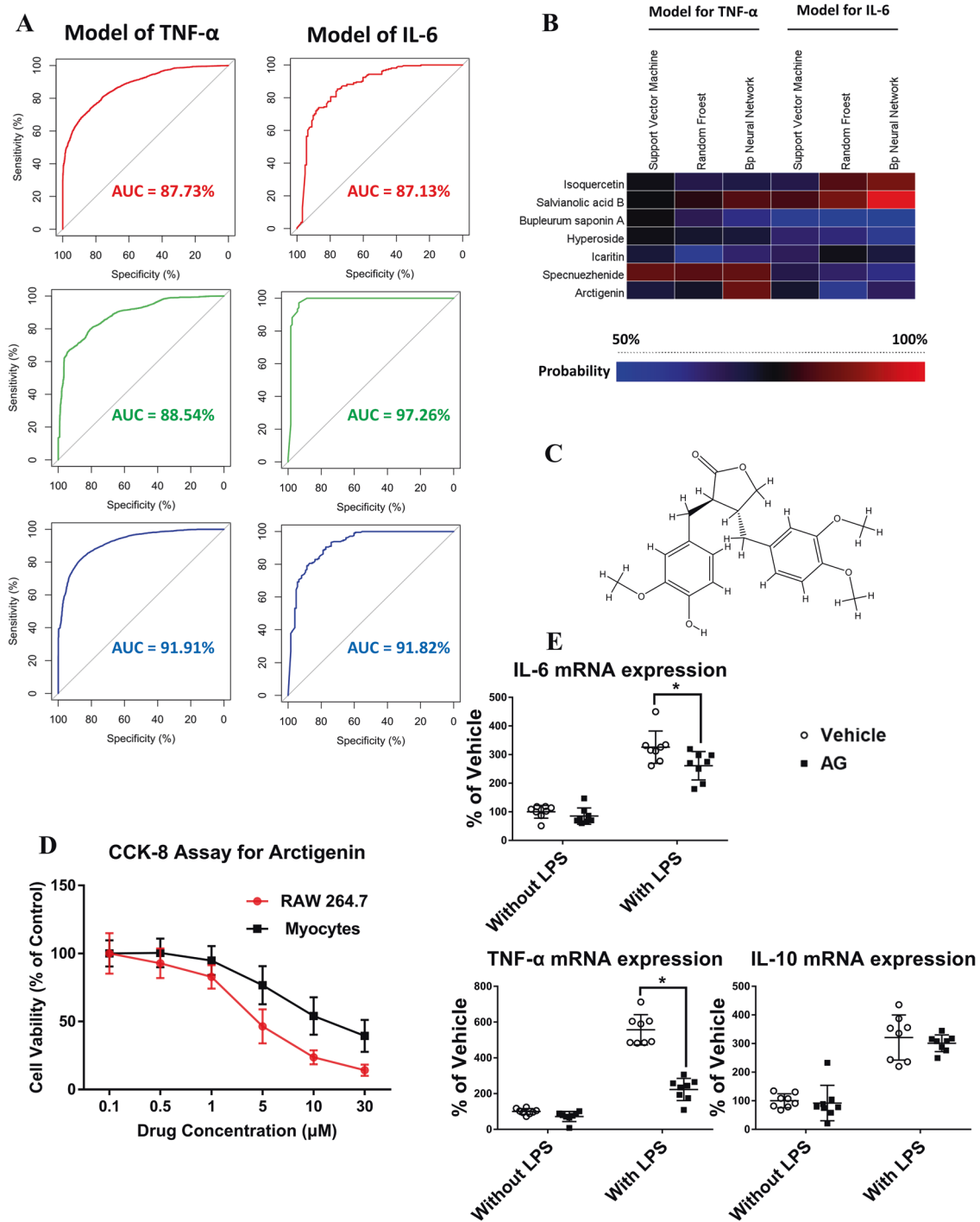
Fig. 1 Prediction of the ability of natural molecules to suppress IL-6 and TNF-α. **a** ROC curves of the three machine learning models (artificial neural network (red), support vector machine (green), and random forest (blue)) through a random tenfold cross-validation. **b** Heatmap of the probability of IL-6 and TNF-α inhibition through machine learning models. **c** Chemical structure of AG. **d** Cellular activity of RAW264.7 cells and cardiomyocytes incubated in various concentrations of AG for 24 h. **e** mRNA levels of cytokines in RAW264.7 cell lines with or without LPS/AG treatment. An asterisk indicates significant difference vs. vehicle

To investigate the detailed mechanism of macrophage polarization modulation, we measured 11 markers in four macrophage subsets. Our results showed that AG significantly decreased the levels of M1 (TLR2 and TLR4) and M2c (TLR1 and TLR8) markers and significantly increased the levels of M2a (CHIL3), M2b (H2-Aa), and M2d (VEGFA) markers ($P < 0.05$, Fig. 2c). Since cytokines from M2 macrophages show multiple antiapoptotic and prosurvival effects, we investigated the apoptosis status of mouse cardiomyocytes after coculture with RAW264.7
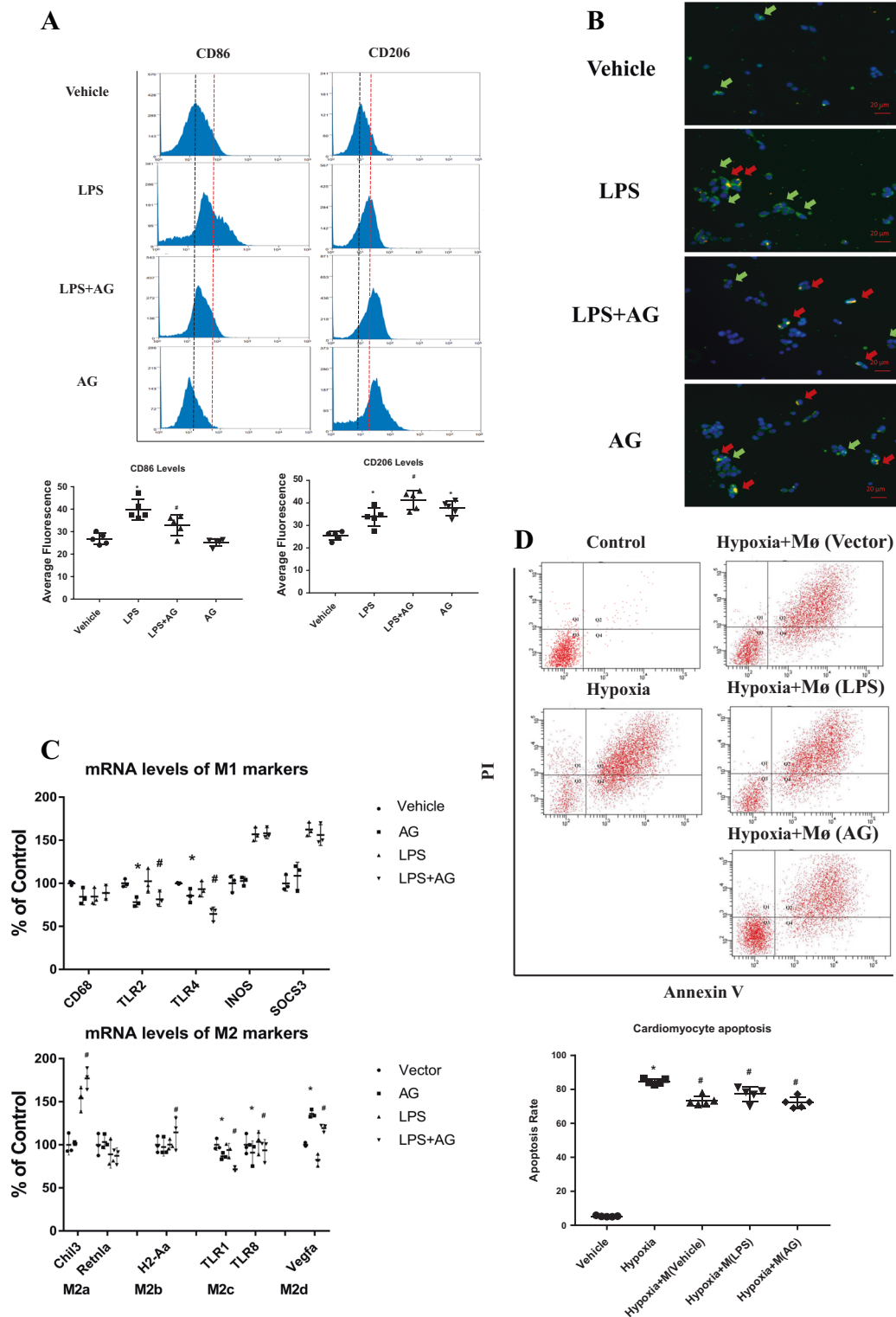
Fig. 2 Effect of AG on macrophage M1/M2 polarization. **a** Representative flow cytometry histograms showing the surface expression of CD86 (an M1 marker) and CD206 (an M2 marker) in RAW264.7 cells (black line, median fluorescence of the vehicle group; red line, median fluorescence of the LPS group). An asterisk indicates significant difference vs. vehicle; a hash indicates significant difference vs. LPS. **b** Immunofluorescence staining of CD86 (green) and CD206 (red) in RAW264.7 cells with or without LPS/AG treatment (magnification,

40×). **c** mRNA levels of M1/M2 polarization markers in RAW264.7 cell lines as determined by qPCR. An asterisk indicates significant difference vs. vehicle; a hash indicates significant difference vs. LPS. **d** Representative flow cytometry profile showing apoptosis among cardiomyocytes cocultured with RAW264.7 cells pretreated with LPS or AG. An asterisk indicates significant difference vs. vehicle; a hash indicates significant difference vs. hypoxia

cells in vitro. Our results showed that the apoptosis percentages of cardiomyocytes were the highest at 89.25%, while those of untreated macrophages, LPS-pretreated macrophages, and AG-pretreated macrophages were lower at 72.12%, 80.17%, and 68.87%, respectively. Although the differences were not obvious, the apoptosis percentages differed between the groups with AG treatment and that with LPS treatment (Fig. 2d, $P < 0.05$). Taken together, our results show that AG could inhibit macrophage M1/M2c polarization and promote M2a/M2b/M2d polarization.

AG alleviates postinfarction cardiac injury

The evidence suggested that upregulating proinflammatory/antiinflammatory factor ratios may protect cells from postinfarction cardiac injury; thus, we tested this hypothesis with in vivo experiments. The treated mice were divided into two groups according to the time of treatment initiation: the AG1

group, which contained the mice that received 2 mg/kg AG 2 h after ligation, and the AG2 group, which contained the mice that received the AG 3 days after ligation. At the beginning, there were 20 mice in each group. Our data showed that over 30 days of treatment, the AG2 group seemed to exhibit fewer death events than the MI-only group (hazard ratio = 0.5841, 95% confidence interval = 0.258–1.324, $P = 0.19$, Fig. 3a), although the difference was not significant. AG improved EF in the AG2 group but not in the AG1 group (Fig. 3b). Histological analysis indicated that infarct size was significantly reduced in the AG2 group but not in the AG1 group compared with the MI-only group ($P < 0.05$, Fig. 3c). We next examined myocardial death using TUNEL staining. The results showed that AG treatment reduced the number of dead cells in both the AG1 and AG2 groups ($P < 0.05$, Fig. 3d). qPCR of heart tissue showed that the mRNA levels of both IL-6 and TNF-α were significantly decreased in the AG1 and AG2 groups compared with the

Fig. 3 Cardioprotective effect of AG on an MI mouse model. **a** Kaplan–Meier survival curves of sham mice and MI mice treated with AG or equal volumes of saline. **b** Echocardiographic measurements of EF in mice 28 days after MI. **c** Representative images and statistical data of heart sections labeled with Masson's trichrome stain and a histogram of the infarct area. **d** Representative images and statistical data of heart sections with TUNEL staining and HRP labeling. **e** mRNA levels of IL-6, TNF-α, and IL-10 in each group of mice. An asterisk indicates significant difference vs. sham; a hash indicates significant difference vs. MI
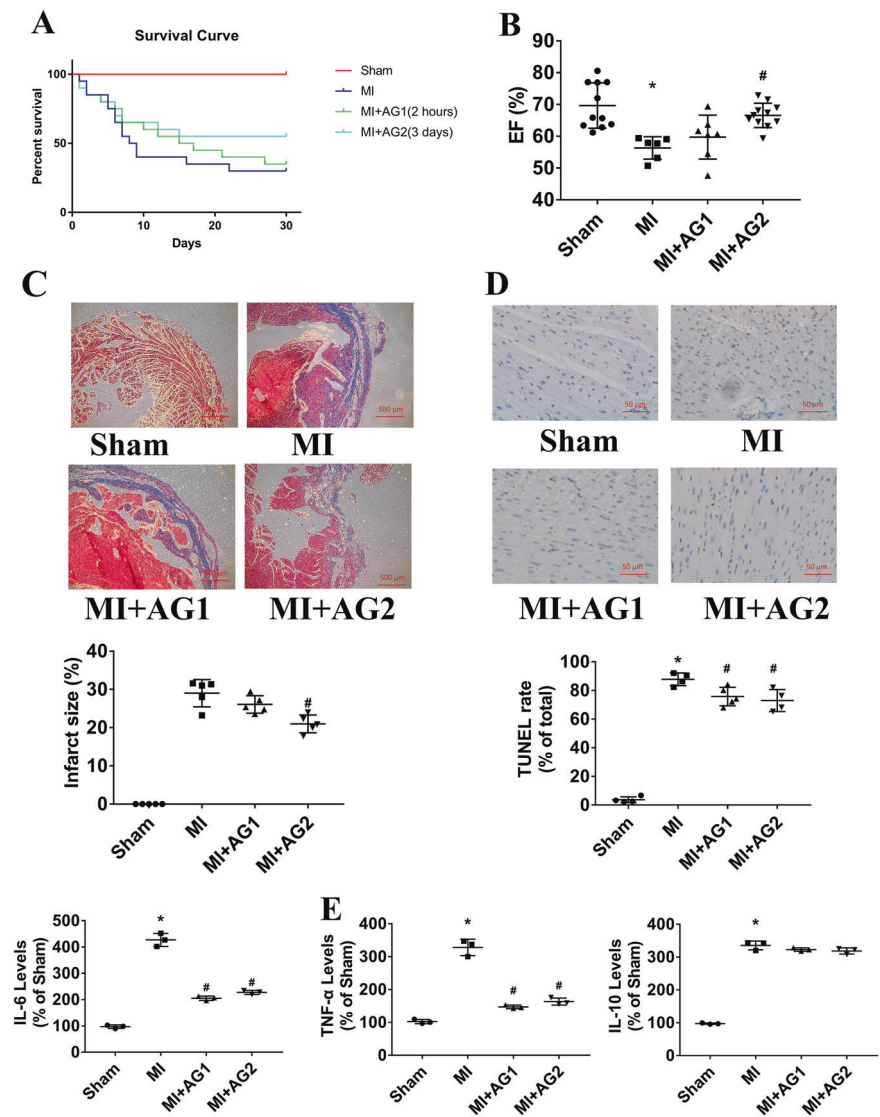
MI-only group ($P < 0.05$), while the IL-10 levels did not differ ($P > 0.05$), suggesting that the cardioprotective effect of AG was more dependent on direct downregulation of inflammatory factors than on upregulation of antiinflammatory factors. Overall, our in vivo data suggest that AG can alleviate postinfarction cardiac injury but that the effect may be impacted by the time of intervention.

AG suppresses inflammatory macrophages in vivo

To investigate the effect of AG on macrophages in cardiac tissue, we examined three markers (CD86, CD206, and CCR2). First, we purified macrophages from heart tissue by FACS based on F4/80 levels (Fig. 4a). We found that the expression of both the CD86 and CD206 markers in heart
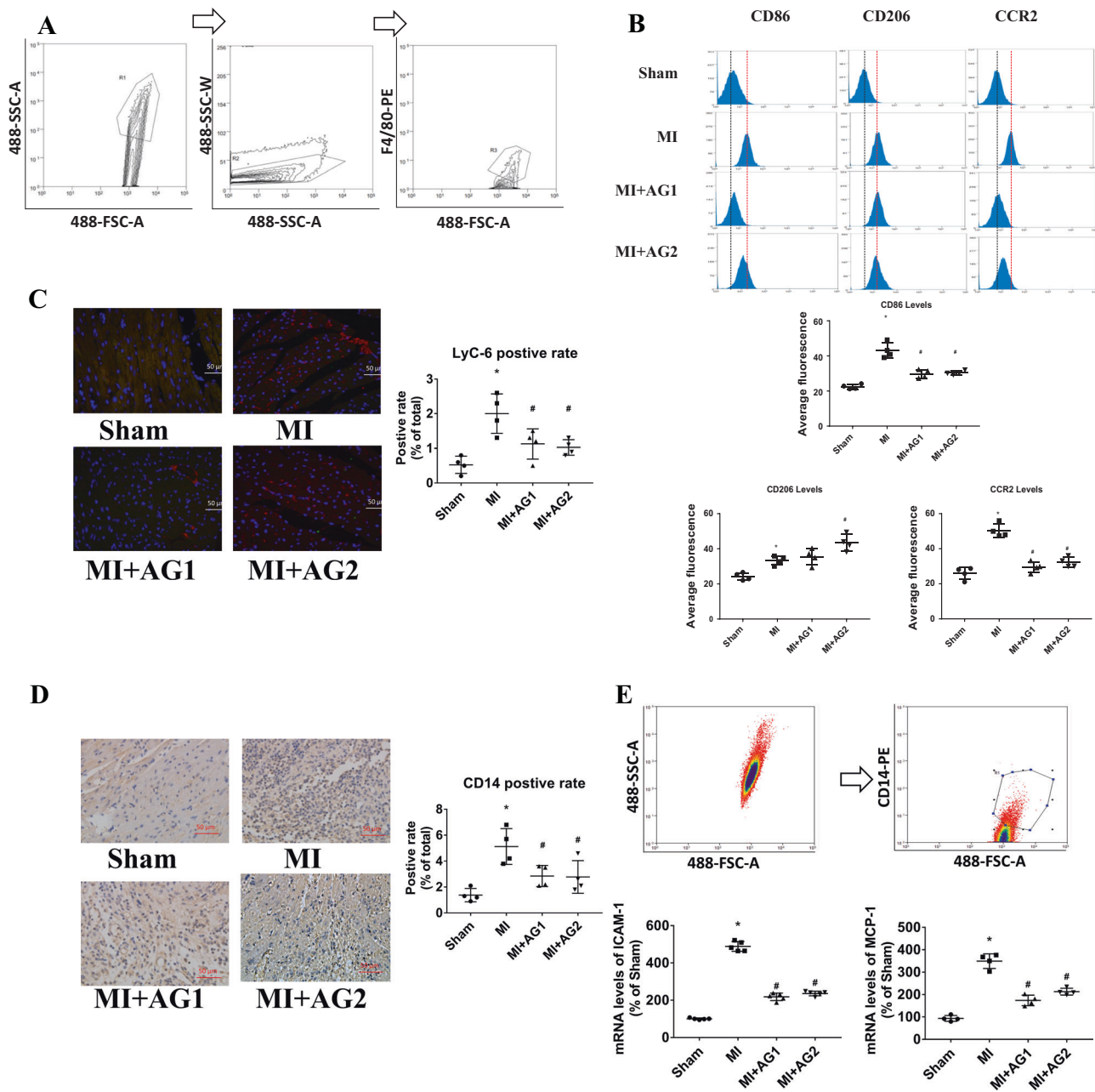

Fig. 4 Effects of AG on cardiac macrophages and monocytes in mice with MI. a Workflow and FACS gating strategy for the separation of cardiac macrophages (F4/80+). b Representative flow cytometry histograms showing the surface expression of CD86, CD206, and CCR in cardiac macrophages (black line, median fluorescence of the sham group; red line, median fluorescence of the MI group) and a statistical histogram of the flow cytometry results. c Representative immunofluorescence staining of LyC6 (red) in heart sections and statistical data. d Representative immunochemical staining of CD14 in infarcted hearts and statistical data. e Workflow and FACS gating strategy for the separation of monocytes (CD14+) in mouse plasma and analysis of the mRNA levels of MCP-1 and ICAM-1 in blood monocytes from each group. An asterisk indicates significant difference vs. sham; a hash indicates significant difference vs. MI

macrophages was increased in the MI-only group compared with the sham group. The expression of the CD206 marker was further increased in the AG2 group, and the expression of the CD86 marker was decreased in the AG1 and AG2 groups ($P < 0.05$, Fig. 4b). In addition, we found that the expression of the CCR2 marker was significantly decreased in the heart macrophages of MI mice that received AG treatment compared with those of MI mice that did not receive AG treatment ($P < 0.05$, Fig. 4b). Given that inflammatory macrophages are mostly derived from LyC6+ monocytes, we detected LyC6 markers by immunofluorescence. The results showed that the numbers of LyC6 + cells were increased in the heart tissues of MI-only mice and were decreased in the heart tissues of AG1 and AG2 mice ($P < 0.05$, Fig. 4c). In addition, the immunohistochemistry results showed that infiltration of myeloid cells (CD14+) was increased in the heart tissues of mice subjected only to MI and decreased in the heart tissues of mice that received AG treatment ($P < 0.05$, Fig. 4d). These results suggested that AG may inhibit the infiltration of plasma myeloid cells into infarcted tissue. Therefore, we sorted monocytes from blood by CD14 labeling and quantified the mRNA levels of two important adhesion molecules (MCP-1 and ICAM-1). The results showed that the mRNA levels of both MCP-1 and ICAM-1 were significantly decreased in the AG1 and AG2 groups compared with the MI-only group (4F, $P < 0.05$). Therefore, our data show that AG could suppress inflammatory macrophages and monocytes in vivo.

NFAT5 is a predicted target of AG

We used RNA-Seq analysis to determine the mechanism of action of AG on macrophages. The GSEA plot from the KEGG database indicated that the AG-induced biological processes included several inflammatory processes (Fig. 5a). Of these, the JAK-STAT and NF-κb signaling pathways are thought to be associated with macrophage polarization (Fig. 5b). Furthermore, we investigated the target of AG by GSEA of immunological gene sets in the MSigDB. We found that the NFAT5 knockout gene set met the filtering criteria ($P < 0.01$, Fig. 5c). Then, we determined the gene expression matrix of NFAT5 knockdown with/without 0.2 mg/mL LPS treatment from the Gene Expression Omnibus (GEO) database (GSE26343) and performed t-SNE analysis with our data (GSE127902). The results showed that macrophages with NFAT5 knockout and those with AG treatment clustered together, which may suggest that the mechanism action of AG is at least partly similar to that of NFAT5 knockout (Fig. 5d). To further predict whether AG directly binds to NFAT5, we utilized the SYBYL-X tool to assess the binding affinity between NFAT5 and AG. The structure of NFAT5 (human) was obtained from the Protein Data Bank (1IMH). The results showed that AG can bind to the NFAT5 DNA-binding domain (Fig. 5e). The docking score of AG for NFAT5 was 7.2, which exceeded those of 80% of the molecules in our chemical library. Taken together, our results suggest that the JAK-STAT and NF-κb signaling pathways may be involved in the mechanism of AG and that NFAT5 may be the target of AG.

AG modulates macrophage polarization via the JAK/STAT and NFAT5-induced NF-κb signaling pathways

We performed further experiments to confirm our in silico predictions. Western blotting showed that the levels of p-JAK2, p-STAT1, p-IKBα, and p-P65 were increased in the cardiac macrophages of the MI-only group and decreased in those of the AG1 group and the AG2 group (Fig. 6a). Notably, the in vitro experiments showed that NFAT5 overexpression reversed the AG-mediated downregulation of p-IKBα and p-P65 but had little effect on p-JAK2 and p-STAT1 expression (Fig. 6b). These results suggested that AG may inhibit NF-κb signaling by inhibiting NFAT5. The reporter gene experiment showed that AG decreased the luciferase activity driven by NFAT5, suggesting that AG directly inhibited the transcriptional activity of NFAT5 (Fig. 6c). Through flow cytometry of RAW264.7 cells, we found that the levels of a macrophage inflammatory marker (CD86) were decreased by AG treatment but that this effect was reversed by NFAT5 overexpression (Fig. 6d). The qPCR data showed that in macrophages (RAW264.7 cells), the levels of TNF-α and IL-6, which were decreased by AG, were restored by overexpression of NFAT5 (Fig. 6e). Similarly, overexpression of NFAT5 also attenuated the decreases in MCP-1 and ICAM-1 levels observed in THP-1 cells (Fig. 6f). These findings suggest that AG suppresses the inflammatory phenotype of myeloid cells by inhibiting NFAT5 and that the mechanism may also involve the JAK/STAT and NF-κb signaling pathways.

NFAT5 overexpression abolishes the influence of AG on postinfarction cardiac injury

To verify whether NFAT5 is the key target for the AG-induced protective effect, we used a model in which NFAT5 overexpression was induced by lentivirus infection (Fig. 7a). The mice received the AG 3 days after ligation. The echocardiographic results showed that NFAT5 overexpression significantly reversed the EF changes in 9 days after coronary ligation ($P < 0.05$, Fig. 7b). The infarct size of cardiac tissue was also increased in mice with NFAT5 overexpression compared with those without NFAT5 expression ($P < 0.05$, Fig. 7c). The TUNEL staining results showed that NFAT5 overexpression increased myocardial
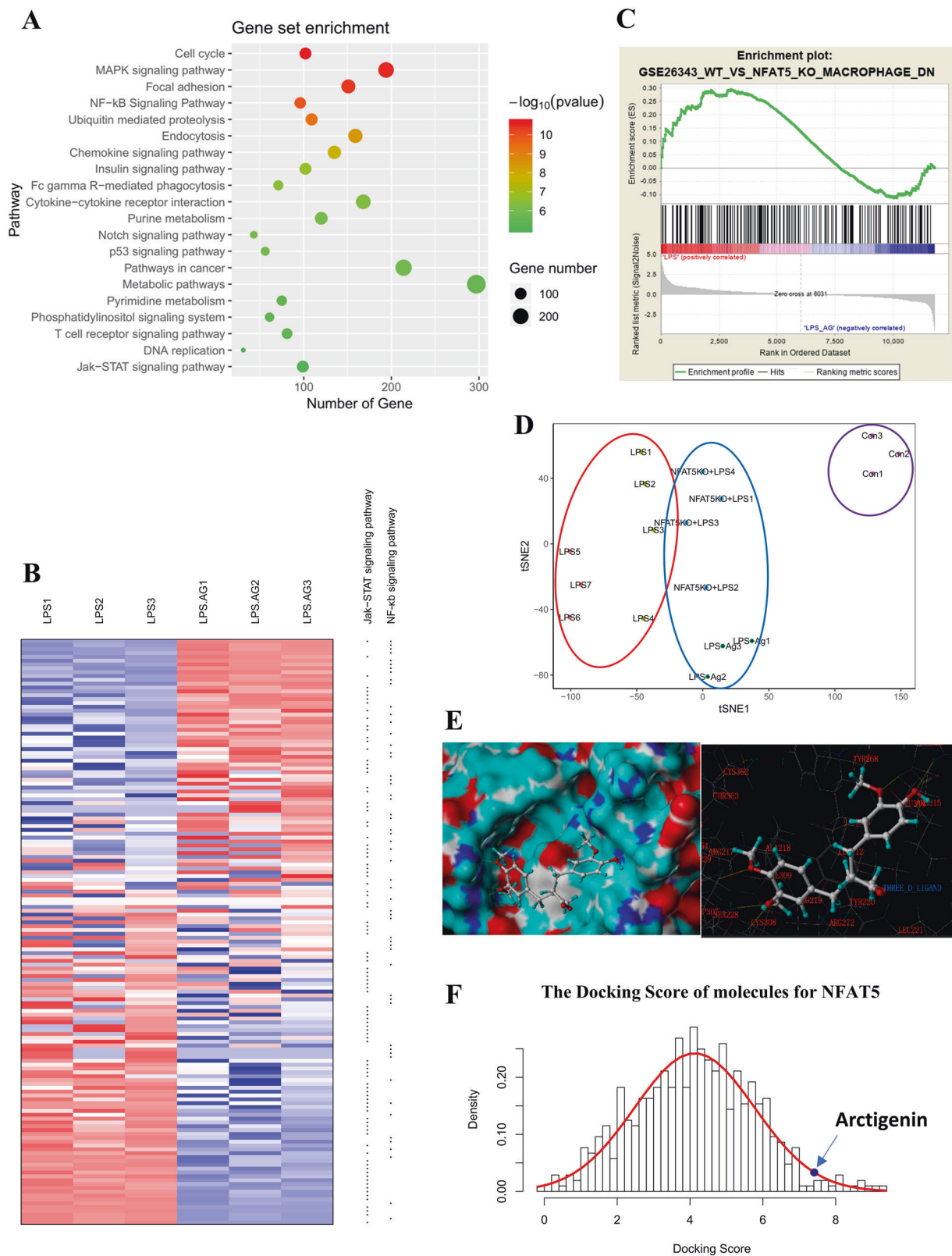
Fig. 5 NFAT5 is predicted to be a key downstream target of AG. **a** KEGG pathway enrichment analysis of genes in macrophages with/without AG treatment. **b** Heatmap of genes involved in the JAK-STAT and NF-κb signaling pathways. **c** GSEA for the immunological signatures of NFAT5-regulated genes in macrophages with/without AG treatment. **d** t-SNE plot showing the distributions of mRNA expression in different samples, including our experimental cells and samples described in the GEO database (GSE26343). **e** Model of the NFAT5 active pocket bound to AG and the residues around small molecules. **f** Distribution of the docking scores of molecules that bound to NFAT5 in our molecular library
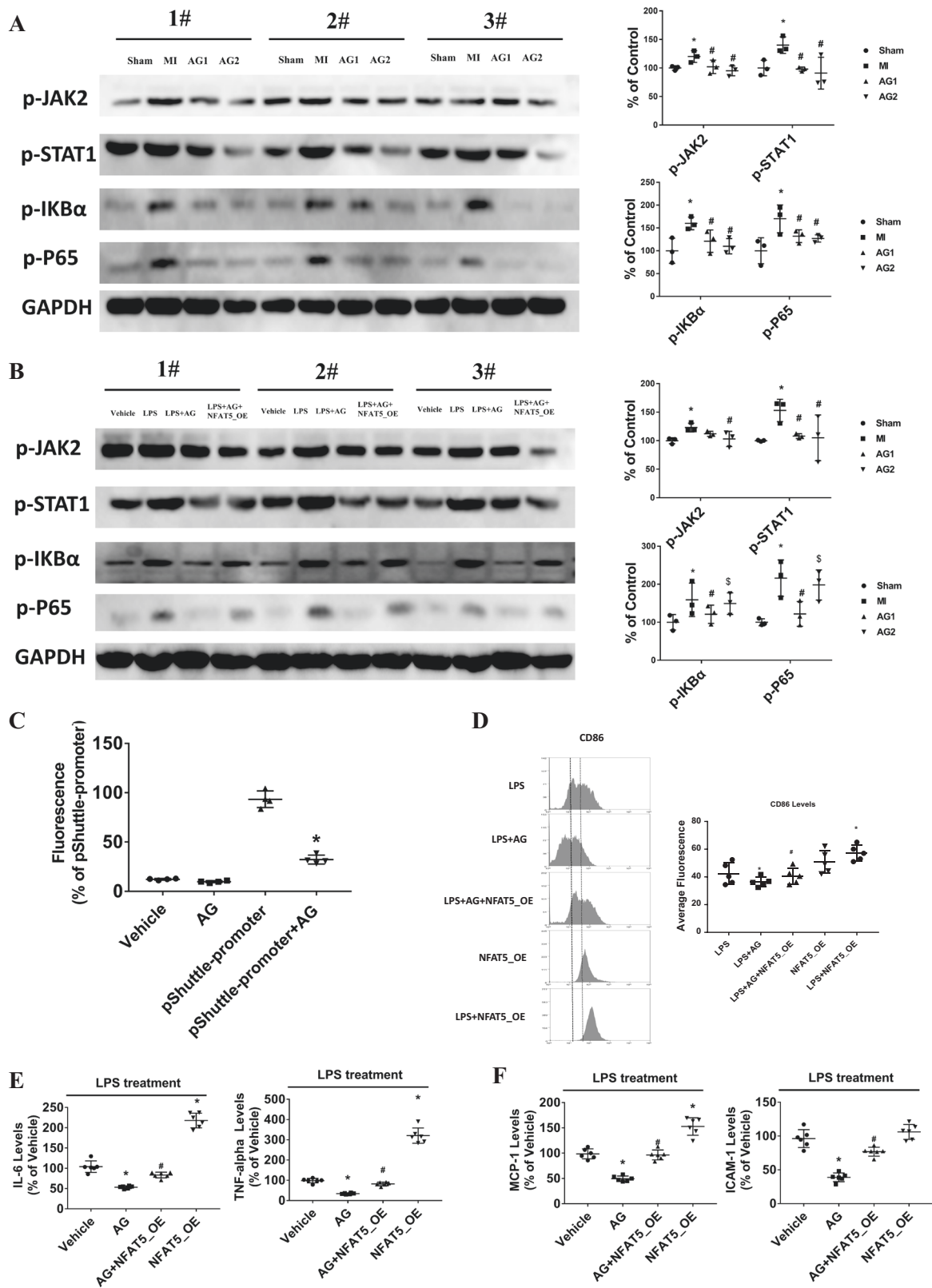
cell death ($P < 0.05$, Fig. 7d). There were no significant differences between MI mice with NFAT5 overexpression and those without NFAT5 overexpression with regard to the echocardiographic and pathological results ($P > 0.05$). We also detected the IL-6 and TNF-α levels in cardiac tissue in the two groups. The qPCR data showed that the levels of

◀ **Fig. 6** AG modulates macrophage polarization via the JAK/STAT and NFAT5-induced NF-κb signaling pathways. **a** Western blotting results showing the levels of phosphorylated JAK2, STAT1, IKBα, and P65 in MI mice with or without AG treatment. An asterisk indicates significant difference vs. sham; a hash indicates significant difference vs. MI. **b** Western blotting results showing the levels of phosphorylated JAK2, STAT1, IKBα, and P65 in RAW264.7 cells treated with LPS, LPS + AG or LPS + AG + lentivirus-OE-NFAT5. An asterisk indicates significant difference vs. vehicle; a hash indicates significant difference vs. LPS; a dollar symbol indicates significant difference vs. LPS + AG. **c** Luciferase activity driven by the NFAT5 motif in macrophages treated with LPS/AG. An asterisk indicates significant difference vs. the pShuttle-promoter. **d** Representative flow cytometry histogram showing the surface expression of CD86 in RAW264.7 cells (red line, median fluorescence of the LPS group; black line, median fluorescence of the LPS + AG group). An asterisk indicates significant difference vs. LPS; a hash indicates significant difference vs. LPS + AG. **e** mRNA levels of IL-6 and TNF-α in the different groups of RAW264.7 cells. **f** mRNA levels of MCP-1 and ICAM-1 in the different groups of RAW264.7 cells. An asterisk indicates significant difference vs. vehicle; a hash indicates significant difference vs. AG

both IL-6 and TNF-α were significantly increased in mice overexpressing NFAT5 compared with those not overexpressing NFAT5 ($P < 0.05$, Fig. 7e). NFAT5 overexpression significantly increased the levels of TNF-α ($P < 0.05$) but had no significant effects on IL-6 ($P > 0.05$). In summary, our findings suggest that NFAT5 is involved in the cardioprotective effect of AG.

Discussion

In this study, we identified that AG, a molecule from a natural product, alleviates heart damage after MI by suppressing the inflammatory myeloid phenotype. Notably, we selected AG from our molecule library through our machine learning strategy and showed that AG can inhibit inflammatory macrophage and monocyte subtypes. Moreover, our results further demonstrated that NFAT5 is involved in the cardioprotective effect of AG and that the JAK/STAT and NF-κb signaling pathways may also be involved in the AG mechanism. Mechanistically, AG suppresses the inflammatory phenotype and decreases proinflammatory factors by inhibiting NFAT5.

Inflammation is thought to be a double-edged sword during the process of MI [20–22]. In the early phase of MI, inflammation promotes tissue necrosis; however, excessive inflammation and delayed repair may lead to poor prognosis [23, 24]. Therefore, many experiments have tried to target the regulation of inflammation, and macrophages play important roles in this process in the heart [25]. Macrophages are the predominant cell type present during inflammation and display functional heterogeneity; normally, proinflammatory macrophages (such as M1 macrophages) initially infiltrate the tissue, after which antiinflammatory and repair macrophages (such as M2

macrophages) are induced. However, this process may be more complex in the heart than in other tissues [26]. Recent studies suggest that the classic M1/M2 classification is not well suited for some pathological processes in the heart [27]. The results of this study showed that macrophages involved in cardiac repair do not conform to canonical M1/M2 programs, as M1/M2 markers were coexpressed in the same cells; thus, the M1/M2 distinction has limited ability to explain the plethora of phenotypes observed in vivo. However, recent mechanistic experiments and drug studies on cardiac macrophages have almost all been based on M1/M2 phenotypes [9, 28, 29]. Therefore, the M1/M2 distinction remains the first choice for most studies until alternative cardiac macrophage markers are found.

Previous studies have defined cardiac macrophage subsets based on the expression of CCR2 and MHCII, which participate in inflammation and fibrotic processes [30, 31]. In our study, we found that AG could decrease the expression of the proinflammatory markers CD86 and CCR2; however, the qPCR results showed that the changes were not always consistent among all markers of M1/M2, suggesting that macrophage subtypes in the heart may need to be further subdivided. In addition, we found that AG also decreased infiltration of LyC6+ and CD14+ cells [31, 32], which are considered to be the precursors of inflammatory macrophages, suggesting that AG can inhibit inflammatory macrophages from both migrating and differentiating. Interestingly, our data show that delayed AG intervention (3 days after ligation) may result in better MI improvement than early AG intervention (2 h after ligation), suggesting that inhibition of inflammation in the early stage may not result in the ideal effect. When and how to regulate the inflammatory process of MI deserve further discussion. In addition, we found that AG could directly reduce myocardial apoptosis in vivo but that the effect was not very obvious in vitro. Although this phenomenon cannot be explained by the existing evidence, we must consider several points. (1) The macrophages in our in vitro experiments were not extracted from an MI environment. Thus, it is possible that these macrophages secreted fewer proinflammatory factors than MI-associated macrophages do in vivo. (2) The experimental system in vitro cannot completely simulate the conditions of ischemia and infarction in vivo. Moreover, the macrophage cell line cannot completely mimic the cardiac macrophage population. (3) In vitro experiments have shown that AG-treated macrophages have a certain antiapoptotic capacity, although the effect is mild.

Several studies have examined the antiinflammatory activity of AG, and AG has also been reported to improve other diseases related to ischemia or ischemia/reperfusion [33–35]. However, the target of AG is still unclear. Our bioinformatic analysis and in vivo experiments showed that
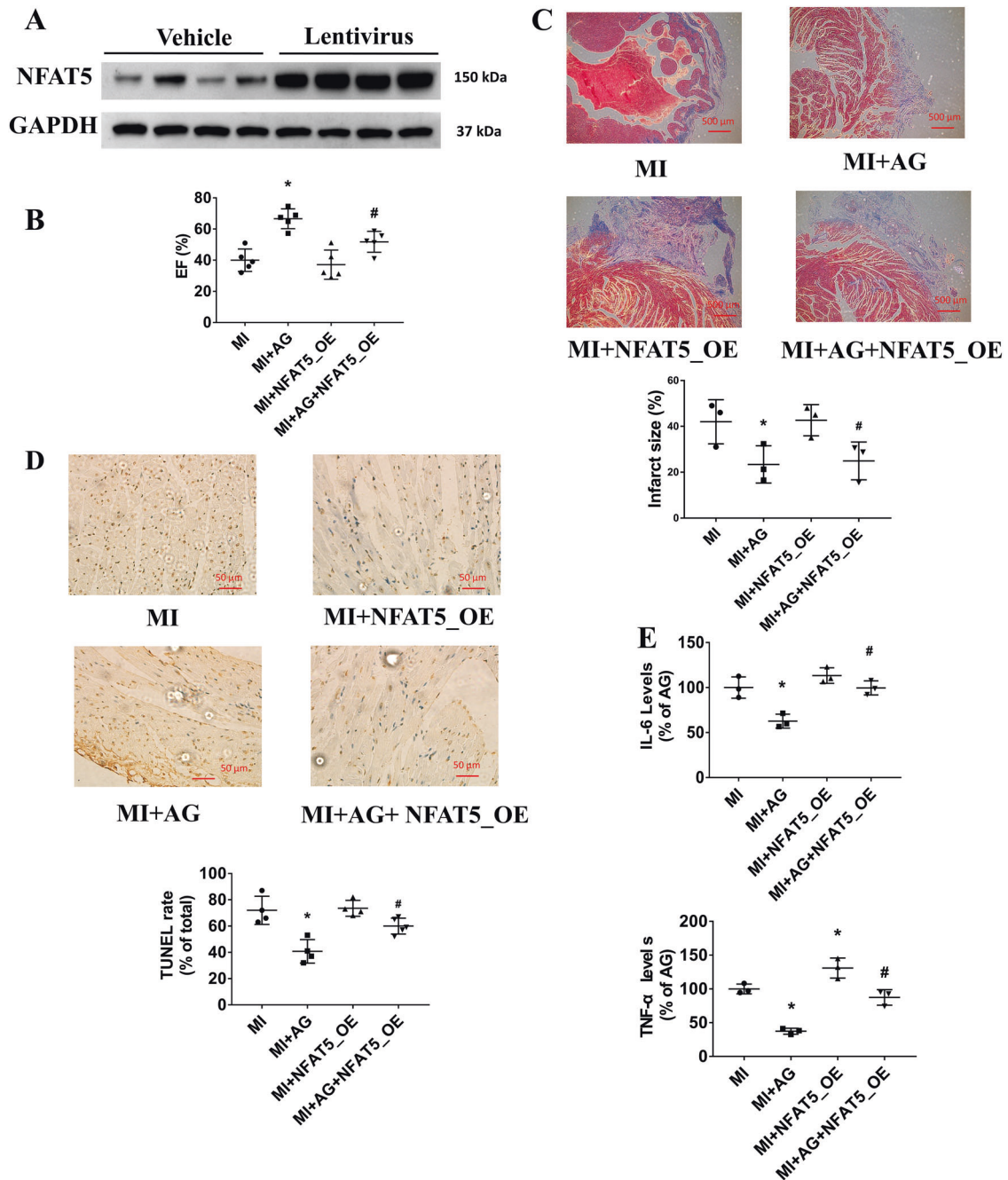
Fig. 7 NFAT5 overexpression reverses the cardioprotective effects of AG. **a** Western blotting results showing the heart tissues of mice with or without lentivirus-OE-NFAT5 injection. **b** Echocardiographic measurements of EF in mice 9 days after MI. **c** Representative images of heart sections labeled by Masson's trichrome stain and a histogram of the infarct area. **d** Representative images of heart sections showing TUNEL staining with HRP labeling. **e** mRNA levels of IL-6 and TNF-α in each group of mice. An asterisk indicates significant difference vs. MI; a hash indicates significant difference vs. MI + AG

NFAT5 may be an important target of AG. NFAT5 is an important transcription factor for immunocyte regulation, which is closely related to the survival and polarization of macrophages and has been implicated in inflammation-related diseases [36–38]. Previous studies have shown that NFAT5 expression in myeloid cells enhances atherosclerosis [39], and our study may expand its function to MI

regulation. Notably, a previous study found that AG reduces inflammatory cell and proinflammatory cytokine infiltration but aggravates ischemia/reperfusion, which can increase apoptosis of tubular cells and induce acute kidney injury [34]. This result may have been due to the high dose used (9 mg/kg). In our study, we did not find marked pathological damage in the livers and kidneys of mice treated with

2 mg/kg AG; however, the balance between the efficacy and toxicity of AG still deserves further attention.

A series of traditional Chinese medicines are used to treat MI in China. More than half of patients are treated with intravenous formulations of traditional Chinese medicine in the first 24 h of hospitalization [12]. However, the complexity of the herbal ingredients makes it difficult to conduct research on their mechanisms and to screen for active ingredients. Recently, computer science has been considered an important and useful tool for the exploration of pharmacology. New compounds with specific and multidimensional features have been identified based on their electrical characteristics (MACCS keys, electrotopological state indices, and PubChem molecular fingerprints). With the development of algorithm science, computer-assisted strategies have greatly increased the efficiency of screening for natural compounds [40, 41]. Docking is the most common method used to predict the preferred orientations for molecular interactions. However, the applicability of this approach is limited when crystallographic parameters are lacking [42]. Machine learning provides a framework for discovering and prioritizing bioactive compounds through "big data" collection. With increases in phenotype and drug data, these algorithms can be utilized to identify the characteristics of compounds, qualitatively and quantitatively distinguish active compounds from inactive compounds with regard to specific phenotypes, and then select compounds with the desired pharmacological effects [43]. We previously attempted to establish our own target-component prediction strategy for mixed natural products [14]. In this study, we collected phenotypic data on natural products, predicted active molecules using our machine learning methods, and identified AG as an ingredient in traditional Chinese medicines that may suppress inflammation and improve MI. These findings provide a foundation for further research on traditional medicines.

Conclusions

In summary, our findings reveal that AG can improve MI by inhibiting the inflammatory phenotypes of macrophages/monocytes. NFAT5 is the target through which AG modulates macrophage polarization via the NFAT5-induced signaling pathway. This finding may lead to the generation of novel therapeutic strategies to improve the prognosis of patients with MI.

Accession number

The data used for high-throughput sequencing have been deposited in the GEO database (GSE127902).

Compliance with ethical standards

References

1. Ruiz-Villalba A, Simon AM, Pogontke C, Castillo MI, Abizanda G, Pelacho B, et al. Interacting resident epicardium-derived fibroblasts and recruited bone marrow cells form myocardial infarction scar. J Am Coll Cardiol. 2015;65:2057–66.

2. Minami E, Castellani C, Malchodi L, Deem J, Bertko K, Meznarich J, et al. The role of macrophage-derived urokinase plasminogen activator in myocardial infarct repair: urokinase attenuates ventricular remodeling. J Mol Cell Cardiol. 2010; 49:516–24.

3. Kang K, Gholizadeh L, Inglis SC, Han HR. Interventions that improve health-related quality of life in patients with myocardial infarction. Qual Life Res. 2016;25:2725–37.

4. White HD, Aylward PE, Huang Z, Dalby AJ, Weaver WD, Barvik S, et al. Mortality and morbidity remain high despite captopril and/or Valsartan therapy in elderly patients with left ventricular systolic dysfunction, heart failure, or both after acute myocardial infarction: results from the Valsartan in Acute Myocardial Infarction Trial (VALIANT). Circulation. 2005;112:3391–9.

5. Chareonthaitawee P, Christian TF, Hirose K, Gibbons RJ, Rumberger JA. Relation of initial infarct size to extent of left ventricular remodeling in the year after acute myocardial infarction. J Am Coll Cardiol. 1995;25:567–73.

6. Gjesdal O, Bluemke DA, Lima JA. Cardiac remodeling at the population level–risk factors, screening, and outcomes. Nat Rev Cardiol. 2011;8:673–85.

7. de Couto G, Liu W, Tseliou E, Sun B, Makkar N, Kanazawa H, et al. Macrophages mediate cardioprotective cellular postconditioning in acute myocardial infarction. J Clin Investig. 2015; 125:3147–62.

8. Heidt T, Courties G, Dutta P, Sager HB, Sebas M, Iwamoto Y, et al. Differential contribution of monocytes to heart macrophages in steady-state and after myocardial infarction. Circ Res. 2014; 115:284–95.

9. Fan Q, Tao R, Zhang H, Xie H, Lu L, Wang T, et al. Dectin-1 contributes to myocardial ischemia-reperfusion injury by regulating macrophage polarization and neutrophil infiltration. Circulation. 2019;139:663–78.

10. Miyazaki T, Otani K, Chiba A, Nishimura H, Tokudome T, Takano-Watanabe H, et al. A new secretory peptide of natriuretic peptide family, osteocrin, suppresses the progression of congestive heart failure after myocardial infarction. Circ Res. 2018; 122:742–51.

11. Ma HD, Deng YR, Tian Z, Lian ZX. Traditional Chinese medicine and immune regulation. Clin Rev Allergy Immunol. 2013; 44:229–41.

12. Spatz ES, Wang Y, Beckman AL, Wu X, Lu Y, Du X, et al. Traditional Chinese medicine for acute myocardial infarction in

western medicine hospitals in China. Circ Cardiovasc Qual Outcomes. 2018;11:e004190.

13. Dong-mei X, Jun-hua Z, Li-yuan K, Ming-jun Z, Hong-cai S. Traditional Chinese medicine for myocardial infarction: an overview. Int J Clin Pract. 2013;67:1254–60.

14. Huang ZY, Wang LJ, Wang JJ, Feng WJ, Yang ZQ, Ni SH, et al. Hispaglabridin B, a constituent of liquorice identified by a bioinformatics and machine learning approach, relieves protein-energy wasting by inhibiting forkhead box O1. Br J Pharmacol. 2019;176:267–81.

15. Savira F, Cao L, Wang I, Yang W, Huang K, Hua Y, et al. Apoptosis signal-regulating kinase 1 inhibition attenuates cardiac hypertrophy and cardiorenal fibrosis induced by uremic toxins: implications for cardiorenal syndrome. PLoS ONE. 2017;12:e0187459.

16. Tian S, Lei I, Gao W, Liu L, Guo Y, Creech J, et al. HDAC inhibitor valproic acid protects heart function through Foxm1 pathway after acute myocardial infarction. EBioMedicine. 2019;39:83–94.

17. Han S, Gu Y, Yang Y, Shang Q, Yao C, Liu W, et al. Plasma dynamics and tissue distribution of arctigenin after subcutaneous injection in rats. J Yantai Univ. 2017;30:22044.

18. Kim D, Langmead B, Salzberg SL. HISAT: a fast spliced aligner with low memory requirements. Nat Methods. 2015;12:357–60.

19. Meldrum KK, Meldrum DR, Hile KL, Burnett AL, Harken AH. A novel model of ischemia in renal tubular cells which closely parallels in vivo injury. J Surg Res. 2001;99:288–93.

20. Liu J, Wang H, Li J. Inflammation and inflammatory cells in myocardial infarction and reperfusion injury: a double-edged sword. Clin Med Insights Cardiol. 2016;10:79–84.

21. Saxena A, Russo I, Frangogiannis NG. Inflammation as a therapeutic target in myocardial infarction: learning from past failures to meet future challenges. Transl Res. 2016;167:152–66.

22. Ni SH, Sun SN, Huang ZY, Huang YS, Li H, Wang JJ, et al. The pleiotropic association between IL-10 levels and CVD prognosis: evidence from a meta-analysis. Cytokine. 2019;119:37–46.

23. Nahrendorf M, Pittet MJ, Swirski FK. Monocytes: protagonists of infarct inflammation and repair after myocardial infarction. Circulation. 2010;121:2437–45.

24. Prabhu SD, Frangogiannis NG. The biological basis for cardiac repair after myocardial infarction: from inflammation to fibrosis. Circ Res. 2016;119:91–112.

25. Cheng Y, Rong J. Macrophage polarization as a therapeutic target in myocardial infarction. Curr Drug Targets. 2018;19:651–62.

26. Mouton AJ, DeLeon-Pennell KY, Rivera Gonzalez OJ, Flynn ER, Freeman TC, Saucerman JJ, et al. Mapping macrophage polarization over the myocardial infarction time continuum. Basic Res Cardiol. 2018;113:26.

27. Walter W, Alonso-Herranz L, Trappetti V, Crespo I, Ibberson M, Cedenilla M, et al. Deciphering the dynamic transcriptional and post-transcriptional networks of macrophages in the healthy heart and after myocardial injury. Cell Rep. 2018;23:622–36.

28. Jung M, Ma Y, Iyer RP, DeLeon-Pennell KY, Yabluchanskiy A, Garrett MR, et al. IL-10 improves cardiac remodeling after myocardial infarction by stimulating M2 macrophage polarization and fibroblast activation. Basic Res Cardiol. 2017;112:33.

29. Shiraishi M, Shintani Y, Shintani Y, Ishida H, Saba R, Yamaguchi A, et al. Alternatively activated macrophages determine repair of the infarcted adult murine heart. J Clin Investig. 2016;126:2151–66.

30. Bajpai G, Schneider C, Wong N, Bredemeyer A, Hulsmans M, Nahrendorf M, et al. The human heart contains distinct macrophage subsets with divergent origins and functions. Nat Med. 2018;24:1234–45.

31. Epelman S, Lavine KJ, Beaudin AE, Sojka DK, Carrero JA, Calderon B, et al. Embryonic and adult-derived resident cardiac macrophages are maintained through distinct mechanisms at steady state and during inflammation. Immunity. 2014;40:91–104.

32. Schloss MJ, Hilby M, Nitz K, Guillamat Prats R, Ferraro B, Leoni G, et al. Ly6C(high) monocytes oscillate in the heart during homeostasis and after myocardial infarction-brief report. Arterioscler Thromb Vasc Biol. 2017;37:1640–5.

33. Yang J, Yin HS, Cao YJ, Jiang ZA, Li YJ, Song MC, et al. Arctigenin Attenuates ischemia/reperfusion induced ventricular arrhythmias by decreasing oxidative stress in rats. Cell Physiol Biochem. 2018;49:728–42.

34. Han F, Xia XX, Dou M, Wang YX, Xue WJ, Ding XM, et al. Arctigenin: a two-edged sword in ischemia/reperfusion induced acute kidney injury. Biomed Pharmacother. 2018;103:1127–36.

35. Fan T, Jiang WL, Zhu J, Feng Zhang Y. Arctigenin protects focal cerebral ischemia-reperfusion rats through inhibiting neuroinflammation. Biol Pharm Bull. 2012;35:2004–9.

36. Tellechea M, Buxade M, Tejedor S, Aramburu J, Lopez-Rodriguez C. NFAT5-regulated macrophage polarization supports the proinflammatory function of macrophages and T lymphocytes. J Immunol. 2018;200:305–15.

37. Choi S, You S, Kim D, Choi SY, Kwon HM, Kim HS, et al. Transcription factor NFAT5 promotes macrophage survival in rheumatoid arthritis. J Clin Investig. 2017;127:954–69.

38. Kim NH, Choi S, Han EJ, Hong BK, Choi SY, Kwon HM, et al. The xanthine oxidase-NFAT5 pathway regulates macrophage activation and TLR-induced inflammatory arthritis. Eur J Immunol. 2014;44:2721–36.

39. Halterman JA, Kwon HM, Leitinger N, Wamhoff BR. NFAT5 expression in bone marrow-derived cells enhances atherosclerosis and drives macrophage migration. Front Physiol. 2012;3:313.

40. Mamgain S, Sharma P, Pathak RK, Baunthiyal M. Computer aided screening of natural compounds targeting the E6 protein of HPV using molecular docking. Bioinformation. 2015;11:236–42.

41. Li J, Zhou N, Liu W, Li J, Feng Y, Wang X, et al. Discover natural compounds as potential phosphodiesterase-4B inhibitors via computational approaches. J Biomol Struct Dyn. 2016;34:1101–12.

42. Moffat JG, Vincent F, Lee JA, Eder J, Prunotto M. Opportunities and challenges in phenotypic drug discovery: an industry perspective. Nat Rev Drug Discov. 2017;16:531–43.

43. Ding H, Takigawa I, Mamitsuka H, Zhu S. Similarity-based machine learning methods for predicting drug-target interactions: a brief review. Brief Bioinform. 2014;15:734–47.